JOURNAL OF GEOPHYSICAL RESEARCH, VOL. 114, D14302, doi:10.1029/2008JD011607, 2009

Observations of speciated atmospheric mercury at three sites in Nevada: Evidence for a free tropospheric source of reactive gaseous mercury

Peter Weiss-Penzias,[1] Mae Sexauer Gustin,[2] and Seth N. Lyman[2]

Received 9 December 2008; revised 24 February 2009; accepted 28 April 2009; published 16 July 2009.

[1] Air mercury (Hg) speciation was measured for 11 weeks (June–August 2007) at three sites simultaneously in Nevada, USA. Mean reactive gaseous Hg (RGM) concentrations were elevated at all sites relative to those reported for locations not directly influenced by known point sources. RGM concentrations at all sites displayed a regular diel pattern and were positively correlated with ozone (O_3) and negatively correlated with elemental Hg (Hg^0) and dew point temperature (T_{dp}). Superimposed on the diel changes were 2- to 7-day periods when RGM concentrations increased across all three sites, producing significant intersite correlations of RGM daily means (r = 0.53–0.76, $p < 0.0001$). During these periods, enhanced O_3 concentrations and lower T_{dp} were also observed. Back trajectories were applied to develop gridded frequency distribution (GFD) plots and determine trajectory residence times (TRT) in specific source boxes. The GFD for the upper-quartile RGM daily means at one site showed a contributing airflow regime from the high-altitude subtropics with little precipitation, while that developed for the lower-quartile RGM concentrations indicated predominantly lower-altitude westerly flow and precipitation. Daily mean TRT in a subtropical high-altitude source box (>2 km and <35°N) explained a component of the daily mean RGM at two sites (r^2 = 0.37 and 0.27, $p < 0.05$). These observations indicate that long-range transport of RGM from the free troposphere is a potentially important component of Hg input to rural areas of the western United States.

Citation: Weiss-Penzias, P., M. S. Gustin, and S. N. Lyman (2009), Observations of speciated atmospheric mercury at three sites in Nevada: Evidence for a free tropospheric source of reactive gaseous mercury, *J. Geophys. Res.*, *114*, D14302, doi:10.1029/2008JD011607.

1. Introduction

[2] Mercury in the atmosphere is present as gaseous elemental Hg (Hg^0; ~95%), reactive gaseous Hg (RGM; thought to exist as $HgCl_2$, $HgOH_2$, $HgBr_2$) and particulate-bound Hg (Hg_p) [*Schroeder and Munthe*, 1998]. There are only a few sites where continuous long-term air Hg concentration and/or speciation data have been collected and in most cases it has been collected at only one location [cf. *Weiss-Penzias et al.*, 2007; *Abbott et al.*, 2008; *Nadim et al.*, 2001; *Slemr et al.*, 2006; *Sigler and Lee*, 2006; *Liu et al.*, 2007; *Temme et al.*, 2004; *Kellerhals et al.*, 2003]. Understanding the spatial and temporal variation of air Hg speciation is important for determining potential Hg deposition and input to ecosystems. Of particular concern are RGM compounds that are considered to have a short atmospheric residence time due to high calculated deposition velocities and water solubility [*Schroeder and Munthe*, 1998; *Lin and Pehkonen*, 1999]. These forms are also considered more bioavailable than Hg^0, due to the fact that they are preferentially methylated in ecosystems [*Krabbenhoft et al.*, 2005].

[3] Several recent manuscripts reporting on air Hg speciation measurements have shown RGM concentrations in the free troposphere to be >200 pg m^{-3} [cf. *Swartzendruber et al.*, 2006; *Sillman et al.*, 2007]. *Swartzendruber et al.* [2006] collected data at the Mt. Bachelor Observatory in Oregon (2.7 km elevation) and based on observed anticorrelations of RGM with CO, Hg^0, and H_2O suggested that elevated RGM concentrations were not due to direct pollution or long-range transport but were produced by oxidation of Hg^0 in the free troposphere. *Selin et al.* [2007] applied the GEOS-Chem model to interpret global observations of atmospheric total gaseous Hg and RGM and predicted increased RGM concentrations with altitude. Their model results suggested a long lifetime of RGM in the upper troposphere and that subsiding air could be a source of this form of Hg to remote sites, especially at high elevations and locations associated with continental deserts such as Nevada.

[1]Department of Environmental Toxicology, University of California at Santa Cruz, Santa Cruz, California, USA.
[2]Department of Natural Resources and Environmental Science, University of Nevada, Reno, Reno, Nevada, USA.

0148-0227/09/2008JD011607$09.00

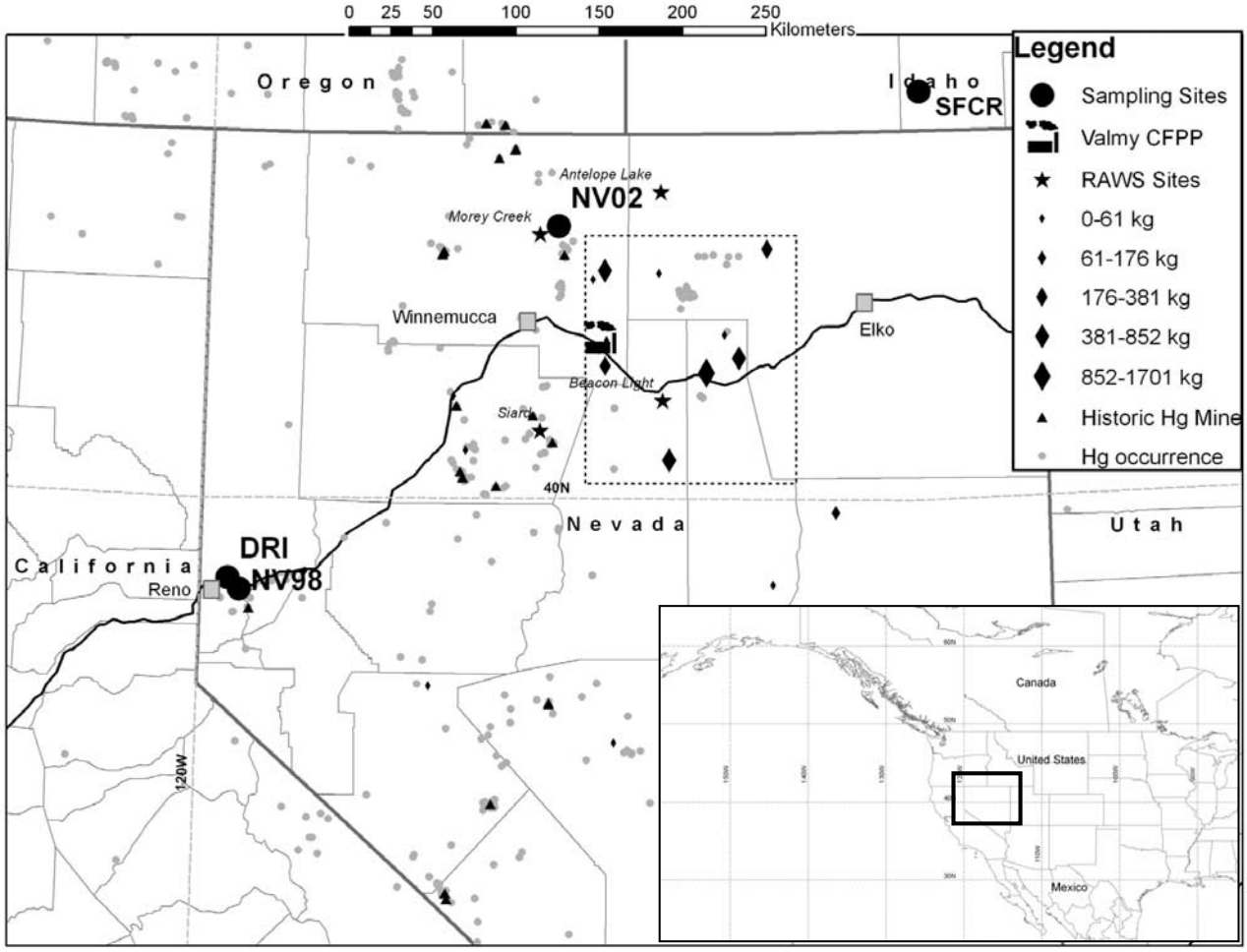

Figure 1. Map showing the locations of the three sampling sites in Nevada, USA (NV02, Desert Research Institute (DRI), and NV98) and the Salmon Falls Creek Reservoir (SFCR) site in Idaho [*Abbott et al.*, 2008]. Also shown are the locations of known geologic deposits of mercury from the U.S. Geological Survey, historic mercury mines, active ore processing facilities from the U.S. Environmental Protection Agency Toxics Release Inventory (sized by total emissions in 2005), and a coal-fired power plant (CFPP). RAWS meteorological sites are shown as black stars. The locations of towns and cities are shown as gray squares. The local source box is denoted by the dotted lines located to the southeast of NV02.

[4] The data presented here are a subset of larger data sets being developed to characterize air Hg speciation in northern Nevada and test the use of surrogate surfaces for determining potential Hg dry deposition. During collection of the data it became apparent that RGM concentrations measured at three study sites in Nevada, including one site quite removed from urban influences, were higher than reported for other rural areas [cf. *Valente et al.*, 2007] and exhibited consistent diel patterns. In addition, periods of high daily average concentrations were correlated across all sites.

[5] On the basis of the above we hypothesized that in situ oxidation of gaseous Hg^0 and convective mixing during the day were providing some RGM measured at all three sites, and a component was derived from the free troposphere. To test our hypothesis we investigated relationships between 2-h and daily averaged concentrations of Hg^0, RGM, and ozone (O_3) and meteorological parameters, and applied back trajectory analyses to determine the source of air interacting with our field sites. Below we discuss the potential factors driving observed diel and longer-term (days) patterns in RGM concentrations.

2. Methods

2.1. Site Description

[6] Data were collected simultaneously at three sites in Nevada, USA for approximately 11 weeks during the summer of 2007. Mercury Deposition Network (MDN) site NV02 (41.50°N, 117.50°W, 1388 m) is situated in a broad, flat desert valley enclosed by the Santa Rosa Range on the west and north, and the Hot Springs Range on the east. Areas of natural Hg enrichment exist within the valley [*Lyman and Gustin*, 2008], and a coal-fired power plant as well as large active gold mines are located to the south and east (Figure 1). Atmospheric Hg and air quality measurements at NV02 were collected at 4 m height, and meteorological measurements were collected at 5 m.

[7] MDN site NV98 (39.51°N, 119.72°W, 1340 m) is located 9 km east of downtown Reno, Nevada on the University of Nevada College of Agriculture, Biotechnology and Natural Resources Experiment Station farm. Reno and the MDN site are situated in a valley with mostly urban and suburban land use (population ~400,000), between the Sierra Nevada and Virginia Mountain ranges. The Reno area has major freeways and rail lines and is home to light industry, however there are no known major anthropogenic atmospheric Hg point sources (U.S. Environmental Protection Agency, Toxics Release Inventory, http://www.epa.gov/triexplorer/). Areas of natural Hg enrichment exist to the north and south of the city [*Coolbaugh et al.*, 2002; *Engle and Gustin*, 2002]. Atmospheric Hg and air quality measurements at NV98 were collected at 4 m, and meteorological measurements were collected at 5 m.

[8] The Desert Research Institute (DRI) (39.57°N, 119.80°W, 1497 m) is also in Reno, Nevada (5 km north of downtown), about 150 m above the valley floor. Atmospheric Hg and air quality measurements at DRI were collected atop a building tower that is 20 m above the ground surface, and meteorological measurements were collected at 15 m. The DRI site is located in the Wedekind Mining District known for gold, silver and Hg deposits [*Garside and Schilling*, 1979]. Air Hg concentrations were monitored by the University of Nevada at this location from 2002 to 2007 [*Stamenkovic et al.*, 2007; *Peterson*, 2009].

2.2. Measurements of Mercury Species

[9] Concentrations of Hg^0, RGM, and Hg_p (<2.5 μm) were measured at all sites with a Tekran 2537A/1130/1135 system [*Landis et al.*, 2002]. The method detection limit (MDL) according to Tekran is 0.1 ng m^{-3} for Hg^0. For RGM and Hg_p, the MDL, calculated as 3 times the standard deviation of the 1130/1135 system blanks, was ~5 pg m^{-3}. Variability of Tekran 2537A Hg^0 and 1130 RGM concentrations between colocated instruments were compared in this study and in others [cf. *Abbott et al.*, 2008; *Landis et al.*, 2002; *Lyman and Gustin*, 2008; *Peterson*, 2009] and may be on the order of 10 and 30%, respectively. These values are important to consider during data comparisons.

[10] The flow rate through the Tekran 1130 and 1135 modules at all sites was 7 standard L min^{-1} (standard conditions of 0°C and 100 kPa), and the flow rate through the Model 2537A was 1 standard L min^{-1}. The system was set for a 2 h RGM sampling and 1 h desorption cycle. The Model 2537A internal permeation source was used to perform automatic calibrations every eight 3 h sampling cycles. The accuracy of the Tekran 2537A internal permeation source was checked every 3 months by injection of saturated Hg vapor air into Hg-free air being sampled by the instrument. Denuders and particulate filters were replaced every 3 weeks. Calibration checks were performed weekly by injecting air saturated with Hg vapor into ambient air being sampled by the instrument. The latter entailed injections of concentrations of ~20 ng m^{-3}, allowing the accuracy of all instruments to be checked with respect to a common standard.

2.3. Ancillary Measurements

[11] At NV02, ozone was measured with a Teledyne-API Model 400E, carbon monoxide with a Teledyne-API Model 300EM, NO_x with a Teledyne-API Model 200E and sulfur dioxide with a Teledyne-API Model 100E. At NV98, ozone was measured with a Teledyne-API Model 400E and sulfur dioxide was measured with a Teledyne-API Model 100E. Calibration checks of the Model 400E were performed weekly using an ozone generator and photometer inside a Teledyne-API Model 700 Dynamic Dilution Calibrator, and the Model 700 was regularly checked against a NIST-traceable ozone standard. Carbon monoxide, sulfur dioxide, and NO_x instruments were calibrated weekly using a standard gas cylinder. At DRI, ozone was measured with a Thermo Model 49. The instrument was checked quarterly against a NIST-traceable ozone standard. According to Teledyne-API (http://www.teledyne-api.com/manuals), the method detection limits (MDLs) for the O_3, SO_2, NO_x, and CO instruments are 0.6 ppb, 0.4 ppb, 0.4 ppb, 0.2 ppm, respectively. The O_3 analyzer at DRI has an MDL of 1 ppb.

[12] A Met One Automatic Weather Monitoring System was used to collect meteorological measurements at NV02. At NV98, wind speed and direction were measured with a Young Model 05305, humidity and temperature were measured with a Vaisala Model HMP45AC, solar radiation was measured with a LI-COR Model LI200X, and precipitation was measured with an ETI Model NOAH-IV. Meteorological values at NV98 were logged as 5 min averages with a Campbell Scientific CR1000 data logger. At DRI, meteorological data were collected as part of a weather station operated by the Western Regional Climate Center (http://www.wrcc.dri.edu). Daily precipitation data was obtained from four sites nearby to NV02 in the Remote Automated Weather Stations (RAWS) network (http://www.raws.dri.edu/index.html) (Figure 1).

2.4. Hybrid Single-Particle Lagrangian Integrated Trajectory Back Trajectories

[13] Five-day atmospheric back trajectories were calculated for NV02 and DRI every 3 h spanning the duration of the campaign using NOAA's Hybrid Single-Particle Lagrangian Integrated Trajectory (HY-SPLIT) model [*Draxler and Hess*, 1997]. Although RGM is a highly surface reactive species, it has been suggested that it could have an extended lifetime of ~5 days in the free troposphere due to lack of surface deposition and cloud removal [*Selin et al.*, 2007]. An ensemble of locations around NV02 and DRI consisting of nine points equally spaced in a 0.5 × 0.5° grid (with the site in the center) and three vertical levels (300, 600, and 900 m above modeled ground level) were used for each starting time. Thus, a total of 216 trajectories or 26,136 hourly intervals (termed "trajectory points") were calculated each day for each site. Meteorological fields were used from the National Center for Environmental Prediction Eta Data Assimilation System (EDAS) (http://www.nco.ncep.noaa.gov/pmb/products/) that has 40 km horizontal resolution and 26 vertical levels. The EDAS spatial domain includes most of North America, but ends in the Pacific Ocean between 135° and 150°W longitude depending on the latitude.

[14] Two semiquantitative trajectory analysis methods were used to determine the likely positions of air masses arriving at the sites: gridded frequency distributions (GFD), and trajectory residence time (TRT). A GFD effectively shows the amount of time that air has spent

Table 1. Summary of Measured Chemical Species From 5 June 2007 to 21 August 2007 for NV02 and NV98 and 13 June 2007 to 21 August 2007 for the Desert Research Institute[a]

Site	N	Mean	σ	Median	Minimum	Maximum
			RGM (pg m^{-3})			
NV02	520	26	26	17	<MDL	143
DRI	468	87	57	73	5.7	401
NV98	556	46	32	37	<MDL	157
			Hg$_p$ (pg m^{-3})			
NV02	520	6	9	4	<MDL	102
DRI	468	10	10	8	<MDL	180
NV98	556	5	4	5	<MDL	55
			Hg^0 (ng m^{-3})			
NV02	918	1.8	1.4	1.4	0.6	18.1
DRI	751	1.2	0.3	1.2	0.6	2.5
NV98	902	1.7	0.6	1.5	0.9	4.6
			O$_3$ (ppbv)			
NV02	903	40.2	12.4	40.8	6.4	71.9
DRI	660	48.1	11.6	48.7	16.4	83.3
NV98	905	40.8	17.6	41.1	1.3	86.7
			NO$_x$ (ppb)			
NV02	648	0.2	1.0	<MDL	<MDL	18.6
NV98[b]						
			SO$_2$ (ppb)			
NV02	772	1.0	0.2	1.0	<MDL	2.5
NV98	728	0.5	0.3	0.4	<MDL	2.1

[a]N refers to the number of 2-h averages. Abbreviations are as follows: DRI, Desert Research Institute; RGM, reactive gaseous Hg.
[b]Not measured.

in a given 1° × 1° region, by averaging the intersection of trajectory points in each grid cell along the paths of an ensemble of trajectories. Mean trajectory altitude and total precipitation (both standard output from the HY-SPLIT model) within each grid cell were also calculated.

[15] TRT was calculated by averaging the number of trajectory points that fell inside a predefined three dimensional source box. Two source boxes for calculating TRT were used in this study: a "local" box (41.6°–39.8°N, 117.3°–115.3°W, and <1 km altitude) which corresponds to an area containing a coal-fired power plant and ore-processing facilities as well as known areas of natural Hg enrichment and legacy mining in Nevada (Figure 1), and a "subtropical high-altitude" (STHA) box (all longitudes <35°N and >2 km altitude). The STHA box was chosen based on the results of comparing the GFDs for upper- and lower-quartile RGM concentrations.

[16] Numerous studies have employed statistical methods of analyzing trajectories to interpret how changes in synoptic weather conditions influence trace gas measurements [cf. *Weiss-Penzias et al.*, 2006; *Kaiser et al.*, 2007]. The uncertainties in the horizontal and vertical dimensions inherent in using trajectories (roughly 20% of the distance traveled) can be by minimized by calculating trajectories at multiple nearby locations and altitudes, thus creating a data set with sufficient statistical power to overcome the main limitations (subgrid processes, turbulent flow, and convection [*Stohl*, 1998; *Stohl et al.*, 2003]). In spite of our overall confidence in the power of trajectories, we used them in this study as a tool to test hypotheses and not as a substitute for a 3-D chemical transport Hg model [e.g., *Seigneur et al.*, 2004; *Selin et al.*, 2008], which was beyond the scope of this work.

3. Results and Discussion

3.1. Overview of Air Hg Speciation Data

[17] The 11-week mean RGM concentrations were 26, 45, and 86 pg m^{-3} at NV02, NV98, and DRI, respectively, with a maximum 2 h value of 401 pg m^{-3} observed at DRI (Table 1). Values were 2–50 times greater than what has been observed at other locations that are not directly influenced by known sources of RGM [*Laurier and Mason*, 2007; *Weiss-Penzias et al.*, 2003; *Malcolm et al.*, 2003; *Lynam and Keeler*, 2005], and are comparable to data from urban/industrial locations [*Liu et al.*, 2007; *Landis et al.*, 2004; *Sheu et al.*, 2002]. Lower RGM values (37±28 pg m^{-3}) were reported at DRI during a 3-month study in the summer of 2005 [*Stamenkovic et al.*, 2007] and during a 2-week study at NV02 during the summer of 2005 (17±12 pg m^{-3}) [*Lyman and Gustin*, 2008].

[18] Mean Hg$_p$ concentrations at the three sites were similar to those measured at nonurban/industrial sites [*Valente et al.*, 2007; *Malcolm et al.*, 2003; *Gabriel et al.*, 2005] and near the detection limit of the instrument (Table 1). Median values of Hg^0 ranged from 1.2 to 1.5 ng m^{-3} and were comparable to those reported for summer data collected in the western U.S. [*Weiss-Penzias et al.*, 2003, 2007; *Abbott et al.*, 2008; *Stamenkovic et al.*, 2007; *Caldwell et al.*, 2006; *Hall et al.*, 2006]. Periodic Hg^0 enhancements up to 18.1 ng/m^3 (2-h mean) were observed at NV02.

[19] Mean and minimum O_3 were significantly higher ($p < 0.001$) at DRI relative to NV02 and NV98. Mean values at NV02 and NV98 were not significantly different while the greatest variability was observed at NV98 (Table 1).

[20] NO_x was only measured at NV02, and for most of the time, concentrations were below detection limit, except for some spikes of short duration. SO_2 concentrations at NV02 were significantly higher ($p < 0.05$) than at NV98, however neither site exhibited 5-min concentrations >4 ppb.

3.2. Diel Cycles

[21] Composite hourly averages derived using the 11 weeks of data from this campaign revealed regular patterns for most species measured (Figure 2). The diel cycle of RGM with maximum near midday and a nighttime minimum has been observed by others [cf. *Laurier and Mason*, 2007; *Poissant et al.*, 2005] and the correlations with sunlight and temperature (Table 2) suggest that these factors are important in influencing Hg speciation. The phase of the RGM diel cycle at each site matched that of O_3, and was the inverse of that found for T_{dp}. Note that at NV02 the RGM and O_3 maximum and the T_{dp} minimum is shifted ~4 h later and the increase and decrease in these parameters, respectively, was of longer duration than observed at the other sites. Because both O_3 enriched and dry air are derived from the free troposphere, this shift potentially indicates that the boundary layer at NV02 contracts in the afternoon more slowly than at the Reno sites, as suggested by a slight lull in wind speed at 1700 LT, at a time when wind speeds at DRI and NV98 were at their

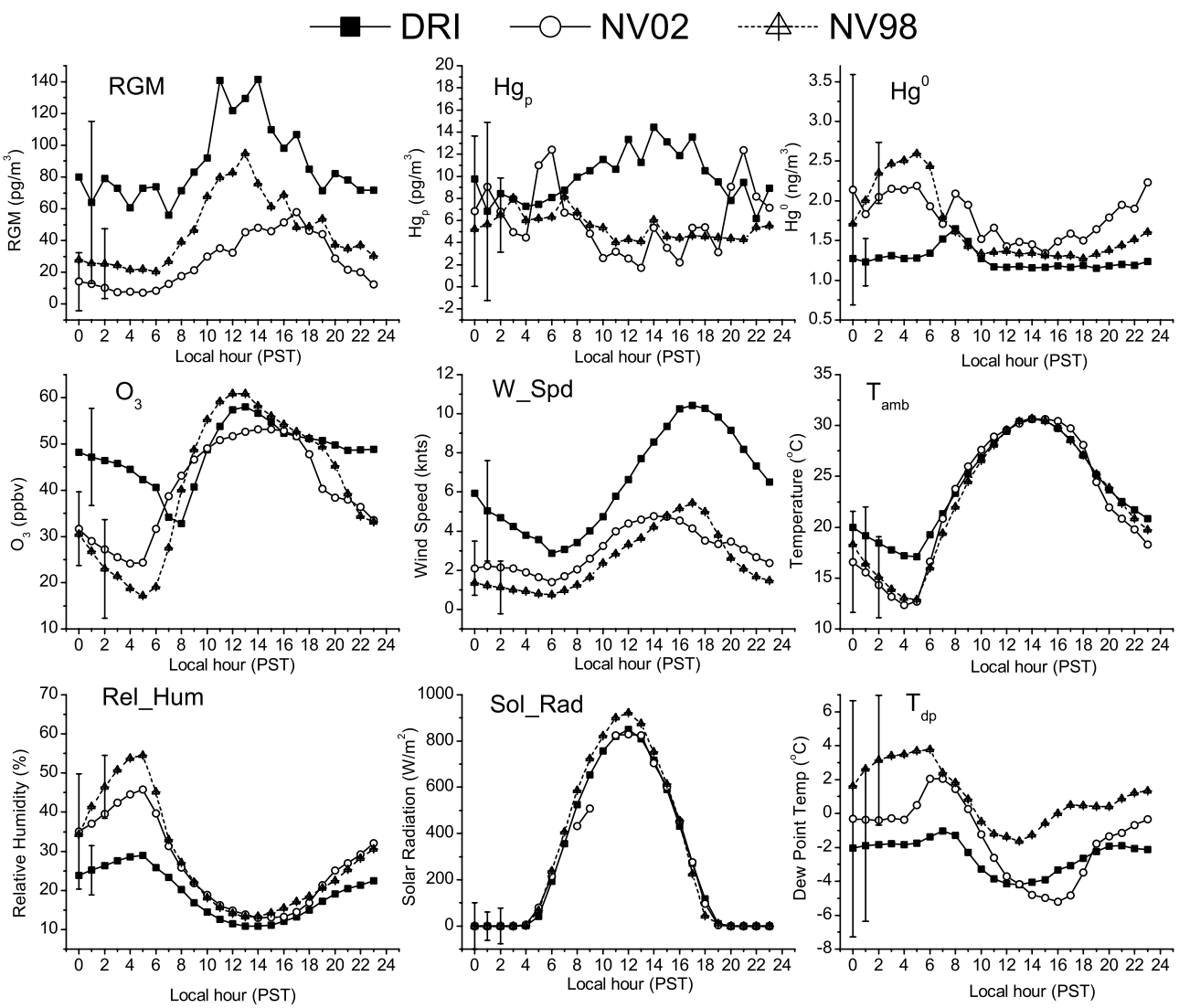

Figure 2. Mean concentrations by time of day for speciated Hg, O_3, and meteorological parameters at three sites. For clarity, only one error bar for each parameter at each site is shown, which represents the mean of each hourly standard deviation (σ). Error bars are shown on hour 0 for NV02, hour 1 for DRI, and hour 2 for NV98.

peak. It could also be argued that the corresponding peaks in both O_3 and RGM at all sites are due to RGM formation occurring via reaction of O_3 with Hg^0. Indeed, the rate constants of *Pal and Ariya* [2004] for this reaction are fast enough to account for the increase in RGM from 0800 to 1600 LT at NV02, but not the diel increase at NV98 or DRI. It is possible that other oxidants such as the hydroxyl radical play a role in forming RGM or as discussed below that the free troposphere is also contributing to observed concentrations. The decline in RGM concentrations in the afternoon may reflect deposition after formation or introduction to the boundary layer. The relatively constant Hg^0 concentrations during the day at all three sites could also indicate mixing in of air from a common source.

[22] The setting of the sites appeared to play a role in the diel cycles of O_3 and Hg species. The O_3 afternoon maximum at NV98 and DRI was enhanced by 5–10 ppb relative to NV02, likely the result of photo-oxidation reactions of locally emitted NO_x and VOCs [*Sillman*, 2003]. The nighttime RGM and O_3 concentrations at DRI were considerably higher and T_{dp} lower than measured at NV02 and NV98, suggesting that this site is situated above the nocturnal boundary layer [cf. *Lin*, 2008]. Similarly, Hg^0 nighttime concentrations were lower at DRI also suggesting that the nocturnal boundary layer is below the elevation of DRI, keeping the site relatively isolated from surface emissions of Hg^0 [*Stamenkovic et al.*, 2007]. As the nocturnal boundary layer broke up in the morning with first light (0700–0900 LT), there was a small but significant peak in Hg^0 accompanied by a steep decline in O_3 at DRI. We speculate that this is not only due to the volatilization of Hg indigenous to the soil in this naturally enriched area and/or reemission of deposited Hg during first light [*Gustin et al.*, 2003; *Engle et al.*, 2001], but also mixing from the boundary layer below of air depleted in RGM and O_3, and enriched in Hg^0.

Table 2. Linear Correlation Coefficients of RGM and Hg^0 With Other Measured Parameters at Two Time Resolutions[a]

	Hg^0	Hg_p	O_3	SO_2	NO_x	T_{amb}	RH	T_{dp}	Sol. Rad.	W. Spd.
					NV02					
RGM	**−0.47**,	**−0.18**,	**0.58**,	*−0.03*,	**−0.13**,	**0.59**,	**−0.65**,	**−0.67**,	**0.37**,	**0.47**,
	−0.49	*−0.07*	**0.36**	**−0.56**	**−0.30**	**0.31**	**−0.73**	**−0.75**	*0.23*	**0.26**
Hg^0	1	**0.15**,	**−0.30**,	**0.14**,	**0.24**,	**−0.27**,	**0.51**,	**0.51**,	**−0.26**,	**−0.29**,
		0.17	*−0.03*	**0.29**	**0.36**	*−0.13*	**0.32**	**0.54**	*−0.05*	**−0.21**
					DRI					
RGM	**−0.32**,	*0.01*,	**0.28**,	–	–	**0.22**,	**−0.57**,	**−0.63**,	**0.31**,	**0.16**,
	−0.33	*0.01*	*0.14*			*−0.08*	**−0.64**	**−0.66**	**0.28**	*0.05*
Hg^0	1	**0.11**,	**−0.18**,	–	–	**−0.10**,	**0.24**,	**0.24**,	**−0.19**,	**−0.35**,
		0.11	*0.22*			*0.11*	*0.21*	*0.23*	**−0.32**	**−0.31**
					NV98					
RGM	**−0.42**,	**−0.19**,	**0.61**,	*−0.15*,	–	**0.63**,	**−0.66**,	**−0.47**,	**0.54**,	**0.35**,
	−0.05	*−0.16*	**0.23**	**−0.31**		**0.32**	**−0.66**	**−0.30**	*0.12*	*0.03*
Hg^0	1	**0.42**,	**−0.57**,	*0.00*,	–	**−0.54**,	**0.71**,	**0.48**,	**−0.36**,	**−0.51**,
		0.54	*0.20*	*0.20*		**0.36**	*0.04*	**0.37**	**−0.31**	**−0.30**

[a]First number is 2-h time resolution; second number is daily time resolution. Coefficients in bold are statistically significant ($p < 0.05$), while those in italics are not.

3.3. Reactive Gaseous Hg (RGM) and Hg^0 Trends Across Three Sites

[23] Daily mean RGM concentrations showed similar major peaks and lows in concentrations across all three sites (Figure 3). Prominent peaks occurred on 22 June, 1 July, 15 July, 6 August, and 13 August, while RGM minima occur on 14 June, 18 July, and 25 July at each of the three sites. Using daily means, significant correlations were found for RGM concentrations between sites (DRI/NV02, r = 0.53; NV98/NV02, r = 0.63; NV98/DRI, r = 0.76; $p < 0.0001$), in contrast with daily Hg^0 concentrations, which were not as well correlated across sites (DRI/NV02, r = 0.27; NV98/NV02, r = 0.16; NV98/DRI, r = 0.06; $p > 0.05$). This observation suggests that regional-scale processes were important in influencing the day-to-day variability of RGM.

[24] Table 2 shows correlations of Hg species with measured parameters at each site at two time resolutions, 2 h and daily. Large enhancement events of Hg^0 concentration occurred at NV02 (Figure 3) on 9 June, 25 July, and 1 August, and these were associated with local precipitation events (discussed below). Because these events skewed the distribution of Hg^0 measurements at NV02 and were not regionally representative, Hg^0 data collected during these periods were not included in the correlation calculations. Consistent positive correlations were found between RGM and O_3, T_{amb}, solar radiation, and wind speed, and negative correlations with Hg_p, Hg^0, RH, and T_{dp}. Hg^0 also displayed consistent correlations: positive with Hg_p, RH, and T_{dp}, and negative with RGM, O_3, T_{amb}, solar radiation, and wind speed. Correlations with RGM at the daily resolution tend to be stronger for RH and T_{dp}, than for the 2-h resolution, suggesting that these are more closely coupled to RGM through synoptic-scale rather than diel changes. Better correlation of RGM with O_3, temperature, and solar radiation at the 2-h resolution suggest that local-scale processes that influence oxidant concentrations are also linked with this form of Hg. The negative correlation of Hg^0 with wind speed suggests that this form may build up in the air under low wind conditions indicating that local surfaces are a source.

[25] If RGM was being directly produced by in situ oxidation of Hg^0 a 1:1 relationship between concentrations

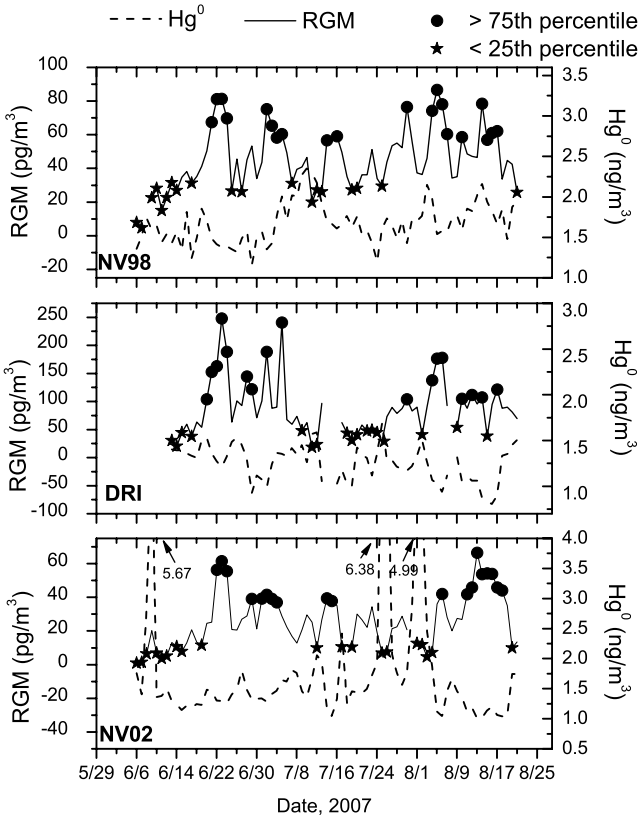

Figure 3. Time series plots of daily mean RGM and Hg^0 concentrations from NV98, DRI, and NV02. Days when RGM concentrations were <25th or >75th percentile of the daily mean distribution are highlighted with symbols. The NV02 Hg^0 plot shows peak daily mean concentrations for the three events that are off-scale.

Table 3. Linear Correlation Coefficients and Slopes of RGM Versus Hg^0 and O_3 at Each Site Using Daily Afternoon Values Corresponding to the Time of Maximum Vertical Mixing Shown in Figure 2[a]

Site	Date Range	RGM/Hg^0	RGM/O_3
NV02	5 Jun–20 Aug 2007	**−0.54**, −65	**0.35**, 1.64
DRI	12 Jun–20 Aug 2007	*−0.16*, −53	*0.16*, 1.10
NV98	5 Jun–20 Aug 2007	**−0.29**, −41	**0.30**, 0.93
NV02	20–25 Jun 2007	**−0.98**, −270	0.07, 0.36
DRI	20–25 Jun 2007	**−0.79**, −510	**−0.37**, −5.8
NV98	20–25 Jun 2007	**−0.57**, −190	−0.06, −0.25

[a]Times are 1200–1600 LT at DRI and NV98 and 1400–1800 LT at NV02. First number is linear correlation coefficient; second number is slope. Data are separated into "all summer data" and "the largest RGM enhancement event," 20–25 June, for each site. Values of r in bold are significant ($p < 0.05$) and those in italics are not. Slopes are in units pg ng^{-1} and pg m^{-3} ppb^{-1} for RGM/Hg^0 and RGM/O_3, respectively.

should be observed during maximum mixing. Similarly if the primary source of RGM is oxidation of Hg^0 in the free troposphere, as suggested by *Swartzendruber et al.* [2006], then a 1:1 relationship between RGM and Hg^0 should also be observed. Table 3 shows calculated correlation coefficients and slopes for RGM versus Hg^0 and O_3 for each site during the time of maximum mixing, as determined using T_{dp}, for all summer data (n = 75) and for the largest RGM enhancement event (20–25 June 2007, n = 6) that occurred across all sites (see Figure 3). If there was a 1:1 relationship with RGM and Hg^0 or O_3 assuming that one is being produced and the other consumed, respectively, the slope would be −1000. The lower slope for RGM/Hg^0 suggests that other processes are influencing the relationship such as deposition of RGM and/or a vertical gradient in Hg^0 due to the surface being a source. The lack of relationship for RGM and O_3 suggests that this reaction is not directly responsible for the observed RGM concentrations whether occurring in the free troposphere or near the surface. For the selected RGM enhancement event (Table 3), the sites displayed stronger RGM/Hg^0 relationships, with slopes closer to the expected limit if RGM and Hg^0 were coupled. This correlation was observed across all sites. The weaker relationship between RGM and O_3 during the high RGM event suggests as mentioned above, that RGM formation through oxidation by O_3 was of limited importance and that atmospheric subsidence and derivation of RGM from the free troposphere was important at this time.

3.4. Local Emissions of Mercury Species

[26] Three major Hg^0 enhancement events were recorded at NV02: 9 June, 25 July, and 1 August (Figure 3) with maximum 5-min Hg^0 concentrations of 12, 28, and 27 ng m^{-3}, respectively. The events were relatively long-lived (mean = 42 h) and displayed their highest concentrations generally between 1900 and 2300 LT, although enhanced values were observed during the day. All events were associated with precipitation in the area around NV02, although none was measured immediately at NV02. Precipitation events have been found to significantly exacerbate Hg emissions from soils [*Lindberg et al.*, 1999] and this response is thought to be due to water displacing Hg bound to soil and soil gas containing Hg [*Gustin and Stamenkovic*, 2005]. This finding is consistent with data collected in 2005 at NV02 that found similar Hg^0 enhancements associated with area thunderstorm activity [*Lyman and Gustin*, 2008] and suggested that increases in air concentrations could be observed across an area where precipitation is occurring and soils are naturally enriched in Hg. Data assessment indicated that these events could not be consistently associated with any anthropogenic point source in the area (mine or coal fired power plant) or biomass burning plumes. For example, background concentrations of SO_2 were observed over the whole time except for a small spike matching Hg^0 on 9 June (event 1). Five-minute concentrations of NO_x reached a maximum value of 16.7 ppb and were correlated with Hg^0 during the second event (r = 0.5, $p < 0.0001$, n = 528) suggesting near field combustion, however, similar results were not seen for events 1 and 3. Trajectory residence times in the local source box (TRT_{local}) (Figure 1) were enhanced for events 1 and 3 but not event 2. Correlations of TRT_{local} with Hg^0, RGM, and Hg_p concentrations on a daily time scale for the entire campaign were also calculated (r = 0.5, −0.2, 0.1, p = 0.0001, 0.2, 0.4, respectively; n = 78), with the stronger correlation with Hg^0 suggesting that this form is locally produced from the local source region, but that RGM and Hg_p concentrations were driven by other forces.

3.5. Free Tropospheric Source of RGM

[27] Superimposed on diel patterns of RGM were periodic multiday enhancements evident across all three sites (Figure 3). In order to examine the chemical and meteorological conditions associated with these high (and low) RGM daily means, the data from each site were segregated by RGM concentration into upper and lower quartiles (Table 4). Back trajectory ensembles were generated for each of these segregated data sets for NV02 to examine the horizontal and vertical air mass locations as well as precipitation along the trajectory paths (Figure 4). Our hypothesis was that when RGM was >75% percentile of the daily mean at the three sites simultaneously, synoptic-scale transport from high altitudes was supplying a component of the RGM.

Table 4. Mean Values of Selected Chemical, Meteorological, and Hybrid Single-Particle Lagrangian Integrated Trajectory Parameters for Data Sets Segregated by RGM Daily Mean Concentration at NV02, DRI, and NV98 From Summer 2007[a]

Percentile	RGM (pg/m^3)	Hg_p (pg/m^3)	Hg^0 (ng/m^3)	O_3 (ppb)	T_{dp} (°C)	TRT_{STHA} (h/traj)
			NV02			
RGM > 75th	47	5	1.2	43	−8.8	24
25th < RGM < 75th	24	7	1.6	41	−2.2	5
RGM < 25th	8	6	2.5	36	4.5	3
			DRI			
RGM > 75th	152	9	1.1	51	−5.9	35
25th < RGM < 75th	80	12	1.3	50	−3.1	22
RGM < 25th	38	10	1.3	45	1.7	13
			NV98			
RGM > 75th	69	4	1.6	41	−0.6	40
25th < RGM < 75th	43	6	1.7	42	1.6	20
RGM < 25th	24	6	1.7	40	2.1	7

[a]Abbreviations are as follows: STHA, subtropical high altitude; TRT, trajectory residence time.

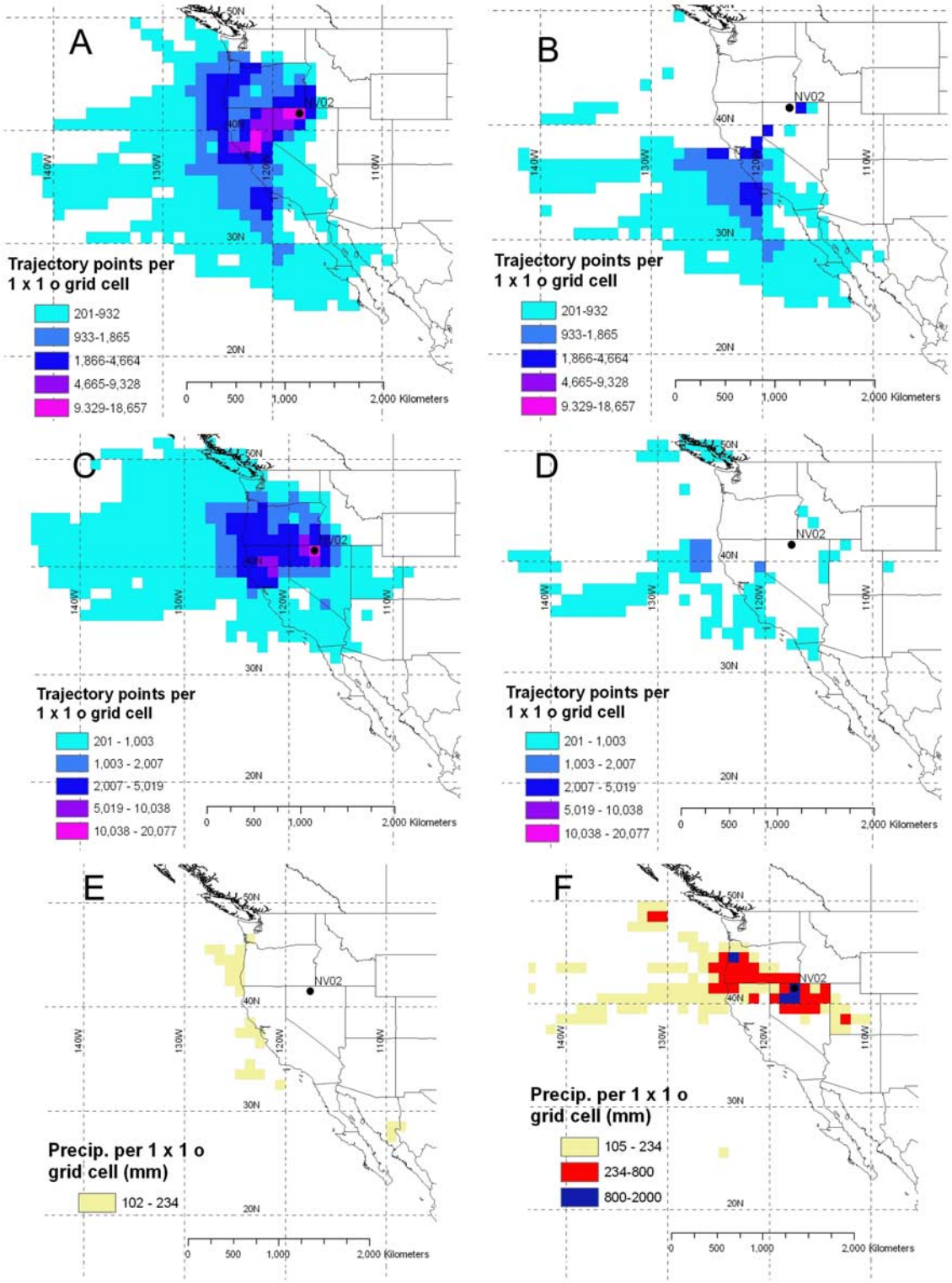

Figure 4. Gridded frequency distributions (GFDs) of back trajectories arriving at NV02 during summer 2007 for two data sets segregated on upper- and lower-quartile mean daily RGM concentrations. Each GFD represents 19 days with 216 trajectories per day for a total of 4104 trajectories, or 492,480 trajectory points. (a) Upper-quartile RGM with grid cells shaded to indicate the frequency of trajectory points occurring in a cell at all altitudes. Only cells with >200 endpoints have been shaded. (b) Same as Figure 4a, except only cells that have >75% of trajectory points > modeled boundary layer height are colored. (c) Lower-quartile RGM with same shading scheme and data exclusion as in Figure 4a. (d) Same as Figure 4b, except lower-quartile RGM. (e, f) Modeled rainfall totals per grid cell for the upper- and lower-quartile RGM concentrations, respectively, with >100 mm/cell shaded.

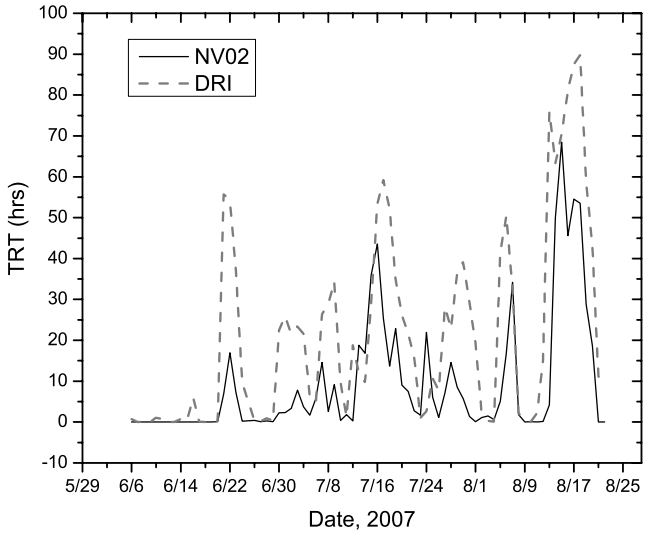

Figure 5. Daily mean trajectory residence times from two starting locations (NV02 and DRI) for the subtropical high-altitude source box.

[28] Table 4 shows that the upper-quartile RGM mean concentrations were associated with lower mean Hg^0 concentrations (significant at NV02 and DRI), higher O_3 concentrations (significant at NV02 and DRI), and lower T_{dp} (significant at all sites). The difference in mean T_{dp} at NV02 between the upper and lower RGM quartiles is especially pronounced (14°C) consistent with the relatively strong RGM/T_{dp} relationship at NV02 in Table 2. Differences in Hg_p values between the upper and lower RGM quartiles were not statistically significant. Hg^0 concentrations at NV02 for the lower RGM quartile were particularly high due to influence from local source emissions associated with precipitation events. No clear pattern in T_{amb} or wind speed was observed between the upper and lower RGM quartiles.

[29] Gridded frequency distributions (GFD) of 5-day back trajectories are shown in Figures 4a and 4c for the upper and lower RGM quartiles at NV02, respectively. Figures 4b and 4d represent the GFD of the upper and lower RGM quartiles, respectively, with shading given to only the grid cells that contain >75% of the trajectory points above the altitude of the top of the modeled mixed layer. Figures 4e and 4f show the total modeled precipitation for each grid cell. High and low RGM days (Figures 4a and 4c) both displayed transport from boundary layer locations to the north and west. However, high RGM days were associated with an arm of transport that is southerly, above the boundary layer and dry (Figures 4b and 4e), whereas low RGM days show very little transport above the boundary layer and have considerable precipitation amounts (Figures 4d and 4f). The southerly arm of transport of dry air from subtropical latitudes was most likely associated with circulation (and subsidence) around a high-pressure system centered over the Arizona, California, and Mexico border region.

[30] On the basis of the results of the GFDs at NV02, trajectory residence times for each site were calculated in a subtropical high-altitude source box (TRT_{STHA}) with boundaries of >2 km altitude and <35°N latitude. These results are shown in Table 4 for the upper, middle, and lower RGM distributions at each site, and in a time series of daily mean TRT_{STHA} values in Figure 5. Table 4 shows that TRT_{STHA} values ranged over a factor of 3–8 between the upper- and lower-quartile RGM data sets, demonstrating the usefulness of this trajectory technique. Figure 5 shows several peaks in TRT_{STHA} that agree in timing with the RGM peaks shown in Figure 3 (e.g., 22 June, 15 July, 6 August, 13 August), though not necessarily in relative magnitudes. Among all upper-quartile RGM days (n = 19), only 2 had TRT_{STHA} < 1 h, whereas for the lower-quartile days 11 of the 19 had trajectories that intersected the STHA box for <1 h. Also, TRT_{STHA} at DRI was consistently larger than at NV02, a pattern that is in agreement with the relative RGM concentrations at DRI relative to NV02. Correlation between daily mean RGM and TRT_{STHA} for the whole campaign was found for each site: DRI (r = 0.25, p < 0.05), NV98 (r = 0.52, p < 0.0001), and NV02 (r = 0.61, p < 0.0001). The relatively weaker correlation at DRI is not fully understood, but may reflect the bias due to missing key data points at DRI when RGM concentrations at NV98 and NV02 were in the upper or lower quartiles.

[31] As a further check of the hypothesis that TRT_{STHA} is a predictor of regional RGM summertime concentrations, trajectories were calculated for NV02 [*Lyman and Gustin*, 2008], DRI [*Peterson et al.*, 2009], and the Salmon Creek Falls Reservoir site in Idaho (SCFR) [*Abbott et al.*, 2008] for previous years. These studies reported lower RGM values than those measured in 2007. Table 5 shows that the average TRT values from these campaigns (using trajectories initialized identically to those in this study) were also lower, providing further support for our hypothesis. Thus, it appears that because the summer of 2007 was abnormally hot and dry [*Peterson et al.*, 2009] and prolonged periods of atmospheric subsidence occurred across Nevada, higher RGM concentrations were observed. Also noteworthy is that during the region's cooler, wetter winter season RGM concentrations were much lower (<10 pg m^{-3}) than those reported here [*Lyman and Gustin*, 2008; *Peterson et al.*, 2009].

4. Conclusions

[32] Mercury species and ancillary parameters were measured simultaneously at three sites in Northern Nevada (NV02, DRI, and NV98) for 11 weeks during the summer

Table 5. Comparison of Mean RGM Concentrations and Trajectory Residence Times in the Subtropical High Altitude Box for the 2007 Data From This Work and Previous Summertime Measurements at Sites in Nevada and Idaho

Site	Year	Dates	Mean RGM (pg m^{-3})	TRT_{STHA}	Reference
NV02	2005	26 Jul–5 Aug	17	7	*Lyman and Gustin* [2008]
SFCR	2005	22 Jul–5 Aug	8.1	5	*Abbott et al.* [2008]
DRI	2006	22 Jul–5 Aug	36	19	*Peterson* [2009]
NV02	2007	6 Jun–21 Aug	26	10	This work
NV98	2007	6 Jun–21 Aug	45	22	This work
DRI	2007	13 Jun–21 Aug	86	24	This work

of 2007. Mean RGM concentrations at all three sites were elevated compared to other rural/suburban locations and also compared to measurements made at the same locations in previous years. RGM displayed a regular diel pattern with a peak around midday and a minimum at night. The phase of this cycle matched that of O_3 and dew point temperature at all three sites suggesting that in addition to in situ photochemical production, convective mixing and entrainment of dry air from the free troposphere during the day was an important contributor to the observed RGM diel pattern. Additionally, superimposed upon this recurring pattern were synoptic-scale periods of enhanced RGM concentrations that occurred at each site more or less simultaneously and produced a significant correlation of RGM daily means between each site (DRI/NV02, $r = 0.53$; NV98/NV02, $r = 0.63$; NV98/DRI, $r = 0.76$; all $p < 0.0001$). At each site (but especially NV02), the upper-quartile RGM daily means were associated with lower Hg^0, elevated O_3, and lower T_{dp}. We suggest that this site, far removed from urban sources of RGM, more clearly showed the influence of free tropospheric additions to the surface. Gridded frequency distributions of back trajectories corresponding to the upper- and lower-quartile RGM concentrations at NV02 showed that on high RGM days, air from subtropical high altitudes was present, indicating that photochemically aged air from upper altitudes was impacting the site. Precipitation along the trajectory paths according to the HY-SPLIT model was virtually nonexistent during high RGM days compared to precipitation occurring across trajectory routes associated with low RGM days. This is consistent with previous modeling of RGM which predicts the accumulation of RGM in cloud-free regions of the upper atmosphere and very low concentrations in the boundary layer in the presence of clouds [*Sillman et al.*, 2007; *Selin et al.*, 2007]. In particular, *Sillman et al.* [2007] showed that, since RGM is extremely soluble and the reactions that produce RGM are relatively slow, air masses need long cloudless periods to accumulate high RGM concentrations. Thus, consistently warm, dry areas like the summertime subtropical high-altitude source box would be a RGM production region in the free troposphere. Trajectory residence times in a subtropical high-altitude region (>2 km altitude and <35°N latitude) were in fair agreement with RGM concentrations at each site, producing statistically significant correlations using daily means. In contrast, TRT_{local} values were weakly negatively correlated with daily mean RGM, but moderately positively correlated with Hg^0, indicating the importance of local sources on Hg^0 but not RGM. Thus, the observed high concentration of RGM at all three sites leads to the possibility that dry deposition of Hg may be exacerbated in rural areas where inputs from the free troposphere occur, potentially impacting ecosystems far from point sources.

[33] **Acknowledgments.** This work was supported by EPRI and EPA STAR grants. Air speciation equipment was loaned to us for this project from EPA Region 9 and ORNL (Steve Lindberg). Special thanks go to Tony and Nancy Lesperance for accommodating our equipment and personnel in their little piece of paradise. Thanks also go to DRI for allowing us to station our air sampling equipment on their roof, with extended thanks to Kyle Ruff for her technical support. Thanks in addition go to William Hafner for providing assistance with the trajectory calculations. We also thank three anonymous reviewers, whose constructive, thoughtful comments were useful for improving the discussion in this article.

References

Abbott, M., C.-J. Lin, P. Martian, and J. Einerson (2008), Atmospheric mercury near Salmon Creek Falls Reservoir in southern Idaho, *Appl. Geochem.*, *23*, 438–453, doi:10.1016/j.apgeochem.2007.12.012.

Caldwell, C. A., P. Swartzendruber, and E. Prestbo (2006), Concentration and dry deposition of mercury species in arid south central New Mexico (2001–2002), *Environ. Sci. Technol.*, *40*, 7535–7540, doi:10.1021/es0609957.

Coolbaugh, M., M. S. Gustin, and J. Rytuba (2002), Annual emissions of mercury to the atmosphere from natural sources in Nevada and California, *Environ. Geol.*, *42*, 338–349, doi:10.1007/s00254-002-0557-4.

Draxler, R. R., and G. D. Hess (1997), Description of the Hysplit_4 modeling system, *NOAA Tech. Memo. ERL ARL-224*, 24 pp.

Engle, M. A., and M. S. Gustin (2002), Scaling of atmospheric mercury emissions from three naturally enriched areas: Flowery Peak, Nevada; Peavine Peak, Nevada; and Long Valley Caldera, California, *Sci. Total Environ.*, *290*, 91–104, doi:10.1016/S0048-9697(01)01068-3.

Engle, M. A., M. S. Gustin, and H. Zhang (2001), Quantifying natural source mercury emissions from the Ivanhoe Mining District, north-central Nevada, USA, *Atmos. Environ.*, *35*, 3987–3997, doi:10.1016/S1352-2310(01)00184-4.

Gabriel, M. C., D. G. Williamson, S. Brooks, and S. Lindberg (2005), Atmospheric speciation of mercury in two contrasting southeastern US airsheds, *Atmos. Environ.*, *39*, 4947–4958.

Garside, L. J., and J. H. Schilling (1979), Thermal waters of Nevada, *Nev. Bur. Mines Geol. Bull.*, *91*, 163 pp.

Gustin, M. S., and J. Stamenkovic (2005), Mercury emissions from soils: Effect of watering and soil water content, *Biogeochemistry*, *76*, 215–232, doi:10.1007/s10533-005-4566-8.

Gustin, M. S., et al. (2003), Atmospheric mercury emissions from mine wastes and surrounding geologically enriched terrains, *Environ. Geol.*, *43*, 339–351.

Hall, B. D., M. L. Olson, A. P. Rutter, R. R. Frontiera, D. P. Krabbenhoft, D. S. Gross, M. Yuen, T. M. Rudolph, and J. J. Schauer (2006), Atmospheric mercury speciation in Yellowstone National Park, *Sci. Total Environ.*, *367*, 354–366, doi:10.1016/j.scitotenv.2005.12.007.

Kaiser, A., H. Sheifinger, W. Spangl, A. Weiss, S. Gilge, W. Fricke, L. Ries, D. Cemas, and B. Jesenovec (2007), Transport of nitrogen oxides, carbon monoxide and ozone to the Alpine Global Atmosphere Watch stations Jungfraujoch (Switzerland), Zugspitze and Hohenpeissenberg (Germany), Sonnblick (Austria) and Mt. Krvavec (Slovenia), *Atmos. Environ.*, *41*, 9273–9287, doi:10.1016/j.atmosenv.2007.09.027.

Kellerhals, M., et al. (2003), Temporal and spatial variability of total gaseous mercury in Canada: Results from the Canadian atmospheric Mercury Measurement Network (CAMNet), *Atmos. Environ.*, *37*, 1003–1011, doi:10.1016/S1352-2310(02)00917-2.

Krabbenhoft, D. P., B. A. Branfireun, and A. Heyes (2005), Biogeochemical cycles affecting the speciation, fate and transport of mercury in the environment, in *Mercury—Sources, Measurements, Cycles and Effects*, edited by M. B. Parsons and J. B. Percival, pp. 139–156, Mineral. Assoc. of Can., Ottawa, Ont., Canada.

Landis, M. S., R. K. Stevens, F. Schaedlich, and E. M. Prestbo (2002), Development and characterization of annular denuder methodology for the measurement of divalent inorganic reactive gaseous mercury in ambient air, *Environ. Sci. Technol.*, *36*, 3000–3009, doi:10.1021/es015887t.

Landis, M. S., G. J. Keeler, K. I. Al-Wali, and R. K. Stevens (2004), Divalent inorganic reactive gaseous mercury emissions from a mercury cell chlor-alkali plant and its impact on near-field atmospheric dry deposition, *Atmos. Environ.*, *38*, 613–622, doi:10.1016/j.atmosenv.2003.09.075.

Laurier, F., and R. Mason (2007), Mercury concentration and speciation in the coastal and open ocean boundary layer, *J. Geophys. Res.*, *112*, D06302, doi:10.1029/2006JD007320.

Lin, C.-H. (2008), Impact of downward-mixing ozone on surface ozone accumulation in Southern Taiwan, *J. Air Waste Manage. Assoc.*, *58*, 562–579.

Lin, C., and S. O. Pehkonen (1999), The chemistry of atmospheric mercury: A review, *Atmos. Environ.*, *33*, 2067–2079, doi:10.1016/S1352-2310(98)00387-2.

Lindberg, S. E., et al. (1999), Increases in mercury emissions from desert soils in response to rainfall and irrigation, *J. Geophys. Res.*, *104*, 21,879–21,888, doi:10.1029/1999JD900202.

Liu, B., G. J. Keeler, J. T. Dvonch, J. A. Barres, M. M. Lynam, F. J. Marsick, and J. T. Morgan (2007), Temporal variability of mercury speciation in urban air, *Atmos. Environ.*, *41*, 1911–1923, doi:10.1016/j.atmosenv.2006.10.063.

Lyman, S. N., and M. S. Gustin (2008), Speciation of atmospheric mercury at two sites in northern Nevada, USA, *Atmos. Environ.*, *42*, 927–939, doi:10.1016/j.atmosenv.2007.10.012.

Lynam, M. M., and G. J. Keeler (2005), Automated speciated mercury measurements in Michigan, *Environ. Sci. Technol.*, *39*, 9253–9262, doi:10.1021/es040458r.

Malcolm, E. G., G. J. Keeler, and M. S. Landis (2003), The effects of the coastal environment on the atmospheric mercury cycle, *J. Geophys. Res.*, *108*(D12), 4357, doi:10.1029/2002JD003084.

Nadim, F., C. Perkins, S. Liu, R. J. Carley, and G. E. Hoag (2001), Long term investigation of atmospheric Hg contamination in Connecticut, *Chemosphere*, *45*, 1033–1043, doi:10.1016/S0045-6535(01)00011-X.

Pal, B., and P. A. Ariya (2004), Studies of ozone initiated reactions of gaseous mercury: Kinetics, product studies, and atmospheric implications, *Phys. Chem. Chem. Phys.*, *6*, 572–579, doi:10.1039/b311150d.

Peterson, C., M. S. Gustin, and S. N. Lyman (2009), Atmospheric mercury concentrations and speciation measured from 2004 to 2007 in Reno, Nevada, USA, *Atmos. Environ.*, doi:10.1016/j.atmosenv.2009.04.053, in press.

Poissant, L., M. Pilote, C. Beauvais, P. Constant, and H. H. Zhang (2005), A year of continuous measurements of three atmospheric mercury species (GEM, RGM and Hgp) in southern Québec, Canada, *Atmos. Environ.*, *39*, 1275–1287, doi:10.1016/j.atmosenv.2004.11.007.

Schroeder, W. H., and J. Munthe (1998), Atmospheric mercury—an overview, *Atmos. Environ.*, *32*, 809–822, doi:10.1016/S1352-2310(97)00293-8.

Seigneur, C., K. Vijayaraghavan, K. Lohman, P. Karamchandani, and C. Scott (2004), Global source attribution for mercury deposition in the United States, *Environ. Sci. Technol.*, *38*, 555–569, doi:10.1021/es034109t.

Selin, N. E., D. J. Jacob, R. J. Park, R. M. Yantosca, S. Strode, L. Jaeglé, and D. Jaffe (2007), Chemical cycling and deposition of atmospheric mercury: Global constraints from observations, *J. Geophys. Res.*, *112*, D02308, doi:10.1029/2006JD007450.

Selin, N. E., D. J. Jacob, R. M. Yantosca, S. Strode, L. Jaeglé, and E. M. Sunderland (2008), Global 3-D land-ocean-atmosphere model for mercury: Present-day versus preindustrial cycles and anthropogenic enrichment factors for deposition, *Global Biogeochem. Cycles*, *22*, GB2011, doi:10.1029/2007GB003040.

Sheu, G.-R., R. P. Mason, and N. M. Lawson (2002), Speciation and distribution of atmospheric mercury over the northern Chesapeake Bay, *ACS Symp. Ser.*, *806*, 223–242.

Sigler, J. M., and X. Lee (2006), Recent trends in anthropogenic mercury emission in the northeast United States, *J. Geophys. Res.*, *111*, D14316, doi:10.1029/2005JD006814.

Sillman, S. (2003), Tropospheric ozone and photochemical smog, in *Environmental Geochemistry, Treatise on Geochem. Ser.*, vol. 9, edited by B. S. Lollar, pp. 407–432, Elsevier, Oxford, U. K.

Sillman, S., F. J. Marsik, K. I. Al-Wali, G. J. Keeler, and M. S. Landis (2007), Reactive mercury in the troposphere: Model formation and results for Florida, the northeastern United States, and the Atlantic Ocean, *J. Geophys. Res.*, *112*, D23305, doi:10.1029/2006JD008227.

Slemr, F., R. Ebinghaus, P. G. Simmonds, and S. G. Jennings (2006), European emissions of mercury derived from long-term observations at Mace Head, on the western Irish coast, *Atmos. Environ.*, *40*, 6966–6974, doi:10.1016/j.atmosenv.2006.06.013.

Stamenkovic, J., S. N. Lyman, and M. S. Gustin (2007), Seasonal and diel variation of atmospheric mercury concentrations in the Reno (Nevada, USA) airshed, *Atmos. Environ.*, *41*, 6662–6672, doi:10.1016/j.atmosenv.2007.04.015.

Stohl, A. (1998), Computation, accuracy and applications of trajectories—a review and bibliography, *Atmos. Environ.*, *32*, 947–966, doi:10.1016/S1352-2310(97)00457-3.

Stohl, A., C. Forster, S. Eckhardt, N. Spichtinger, H. Huntrieser, J. Heland, H. Schlager, S. Wilhelm, F. Arnold, and O. Cooper (2003), A backward modeling study of intercontinental pollution transport using aircraft measurements, *J. Geophys. Res.*, *108*(D12), 4370, doi:10.1029/2002JD002862.

Swartzendruber, P., D. A. Jaffe, E. M. Prestbo, J. E. Smith, P. Weiss-Penzias, N. E. Selin, D. J. Jacob, R. J. Park, S. Strode, and L. Jaegle (2006), Observations of reactive gaseous mercury at the Mt. Bachelor Observatory, *J. Geophys. Res.*, *111*, D24301, doi:10.1029/2006JD007415.

Temme, C., R. Ebinghaus, J. W. Einax, A. Steffen, and W. H. Schroeder (2004), Time series analysis of long-term data sets of atmospheric mercury concentrations, *Anal. Bioanal. Chem.*, *380*, 493–501, doi:10.1007/s00216-004-2715-x.

Valente, R. J., C. Shea, K. Lynn Humes, and R. L. Tanner (2007), Atmospheric mercury in the Great Smoky Mountains compared to regional and global levels, *Atmos. Environ.*, *41*, 1861–1873, doi:10.1016/j.atmosenv.2006.10.054.

Weiss-Penzias, P., D. Jaffe, A. McClintick, E. Prestbo, and M. Landis (2003), Gaseous elemental mercury in the marine boundary layer: Evidence for rapid removal in anthropogenic pollution, *Environ. Sci. Technol.*, *37*, 3755–3763, doi:10.1021/es0341081.

Weiss-Penzias, P., D. A. Jaffe, P. Swartzendruber, J. B. Dennison, D. Chand, W. Hafner, and E. Prestbo (2006), Observations of Asian air pollution in the free troposphere at Mount Bachelor Observatory during the spring of 2004, *J. Geophys. Res.*, *111*, D10304, doi:10.1029/2005JD006522.

Weiss-Penzias, P., D. A. Jaffe, P. Swartzendruber, W. Hafner, D. Chand, and E. Prestbo (2007), Quantifying Asian and biomass burning sources of mercury using the Hg/CO ratio in pollution plumes observed at the Mount Bachelor Observatory, *Atmos. Environ.*, *41*, 4366–4379, doi:10.1016/j.atmosenv.2007.01.058.

M. S. Gustin and S. N. Lyman, Department of Natural Resources and Environmental Science, MS 370, University of Nevada, Reno, Reno, NV 89557, USA. (mgustin@cabnr.unr.edu)

P. Weiss-Penzias, Department of Environmental Toxicology, University of California at Santa Cruz, 1156 High Street, Santa Cruz, CA 95064, USA.